Landslides (2016) 13:1421–1434
DOI 10.1007/s10346-016-0682-x
Received: 14 July 2015
Accepted: 1 February 2016
Published online: 26 February 2016

James T. Kirby · Fengyan Shi · Dmitry Nicolsky · Shubhra Misra

The 27 April 1975 Kitimat, British Columbia, submarine landslide tsunami: a comparison of modeling approaches

Abstract We present numerical simulations of the April 27, 1975, landslide event in the northern extreme of Kitimat Arm, British Columbia. The event caused a tsunami with an estimated wave height of 8.2 m at Kitimat First Nations Settlement and 6.1 m at Clio Bay, at the northern and southern ends of Kitimat Arm, respectively. We use the nonhydrostatic model NHWAVE to perform a series of numerical experiments with different slide configurations and with two approaches to modeling the slide motion: a solid slide with motion controlled by a basal Coulomb friction and a depth-integrated numerical slide based on Newtonian viscous flow. Numerical tests show that both models are capable of reproducing observations of the event if an adequate representation of slide geometry is used. We further show that comparable results are obtained using estimates of either Coulomb friction angle or slide viscosity that are within reasonable ranges of values found in previous literature.

Keywords Landslide tsunami · Coupled slide-tsunami model

Introduction

Landslide-generated tsunamis are a frequent feature of coastlines characterized by complex channel and fjord systems. Bornhold et al. (2001) have provided an overview of landslide-generated tsunamis occurring along the coast of British Columbia and Alaska, and have catalogued events including submarine and subaerial slides. Submarine slide events occurring close to shore often occur at or near low tide when the submarine deposits experience an excess of pore pressure. Resulting slides may be seismically triggered (Rogers 1980), or, in some instances, are possibly triggered by human activities such as pile driving or construction (see the discussion of the 1994 Skagway Harbor, Alaska, event by Kulikov et al. 1996). Slides may also originate subaerially in the form of rockfalls or slumps of saturated soils. Subaerial slides have led to tsunami events of startling magnitude in the BC/Alaska region. The most well known event was the seismically triggered rockfall in Lituya Bay, AK, in 1958, which generated local runups of up to 525 m on the opposing shore (Miller 1960). Bornhold et al. (2007) have documented a case of the apparent destruction of the sizeable First Nation village of Kwalate, in Knight Inlet, as the result of a rockslide-generated tsunami. Thomson et al. (2012) have investigated the potential for large landslide-generated tsunamis in Douglas Channel, BC, using a modeling approach similar to that used in this study.

This study focuses on the landslide event of 27 April 1975 in the northern extreme of Kitimat Arm, British Columbia. The event caused a tsunami with an estimated crest-to-trough height of 8.2 m at the Kitimat First Nations Settlement, and damaged a number of facilities around the shoreline of the upper extent of Kitimat Arm (Fig. 1). Two simulation approaches are employed: an approach treating bottom deformations as solid slides with water column motion induced through the kinematic bottom boundary condition, and an approach which treats slides as a depth-integrated layer of Newtonian viscous fluid, coupled kinematically and dynamically to the upper water layer. The aims of the present study are to examine the aspects of slide geometry controlling observed tsunami behavior and to determine whether a good reproduction of observed results is obtained using reasonable choices of rheological properties in each modeling approach.

The paper is organized as follows. Observational evidence and prior modeling experience are described in "Observations of the 27 April 1975 Kitimat event" and "Modeling background," respectively. "Numerical approach" provides a description of the models being used. "Hindcast of the 1975 Kitimat landslide tsunami" presents results of the model study and comparisons to the observational database. Conclusions are presented in "Discussion."

Observations of the 27 April 1975 Kitimat event

A physical description of events associated with the landslide tsunami of April 27, 1975, may be found in Golder (1975), Murty (1979), and Murty and Brown (1979). Golder Associates reports eyewitness accounts indicating that the event was first noticeable as a failure of a shore-attached breakwater at the northern end of an area known as Moon Bay (Fig. 1). The event spread along the shore of Moon Bay over the course of 2 min, generating a wave that spread out and impacted other sites including the Northland Navigation Wharf, the Eurocan Terminal, and the Kitimat First Nations Settlement across Kitimat Arm. The slide was reported to have occurred about 2 h after lower low water on a large tide (with a local tide range up to 6.2 m). Oscillations of water across the inlet were reported to have persisted for up to an hour. Finally, a wave height of 7.6 m was reported at the First Nations Settlement, based on observed water marks on pilings. Based on comparisons of bathymetric data from before and after the event, Golder (1975) estimated that a slide originated in Moon Bay with a volume of 2.3×10^6 m^3. The slide left a landward scarp extending 183 m along the Moon Bay shoreline. Murty (1979) and Murty and Brown (1979) report additional observations which add to (and in some cases differ from) the initial report of Golder Associates. In particular, it was reported that the event started at 10:05 hours, 53 min after low tide. Two or three waves are said to have occurred at First Nations Settlement, and the maximum crest-to-trough wave height is reported as 8.2 m. Murty and Brown (1979) report an observation that the bottom became exposed at 10:15, 10 min after the start of the event, but where this occurred or the location from where it was observed is not stated. There were additional reports of large waves moving to the south from the event, with one boater visually estimating a wave height of 6.1 m at Clio Bay (location shown in Fig. 6). Based on extensive examination of hydrographic charts, Murty (1979) reported that the total volume of mobilized sediment during the event may have been as large as 2.7×10^7 m^3,

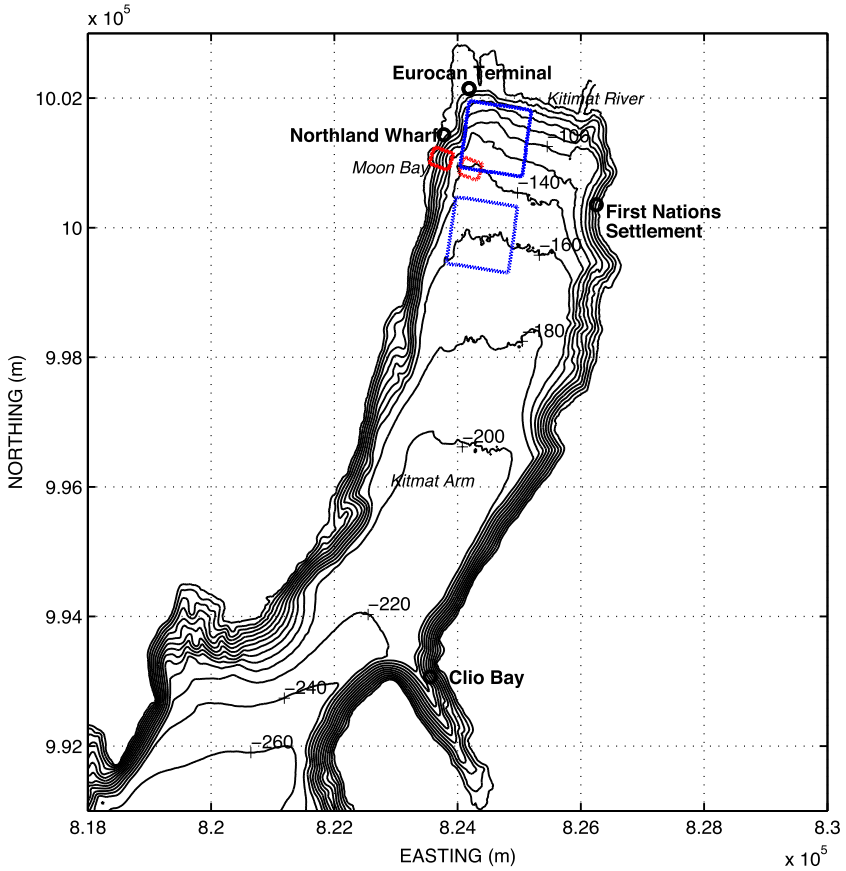

Fig. 1 Northern portion of Kitimat Arm, showing the location of Northland Wharf, Eurocan Terminal, and First Nation Settlement cited in the text. *Solid and dashed red boxes* indicate the initial and final footprints of Moon Bay slide volumes, respectively. *Solid and dashed blue boxes* indicate the initial and final footprints of Kitimat River delta slide volumes, respectively. Final positions are representative of the nondeforming, solid slide computations

or almost ten times as large as the slide volume reported by Golder (1975).

In a series of papers, Prior et al. (1982a; 1982b; 1984) have provided a detailed description of a complex depositional pattern on the floor of Kitimat Arm, resulting from a history of repeated slide events. Readers are referred to these papers for an overview of the geometry, geological setting, and characteristics of slide deposits. Prior et al. examined depositional structures which mainly extend southward from the deltaic formation of the Kitimat River and lie along the central axis of Kitimat Arm. Prior et al. (1984) provide a detailed analysis of the likely progression of the event, with initiation of motion due to failure of the fjord wall (Moon Bay) and then the deltaic front, followed by extensive mobilization of fjord bottom sediment and elongation of the deposit. Prior et al. (1984) estimate the total sediment volume associated with the failure of the river delta structure to be about 2.7×10^7 m^3, but do not attribute this total volume to the 1975 event alone. This volume estimate is consistent with the earlier estimate by Murty (1979) but is not associated only with the initial Moon Bay failure.

Modeling background

Skvortsov and Bornhold (2007) have conducted a model study using a two-layer model consisting of a model based on the nonlinear shallow water equations (NLSWE) for the upper water layer and a depth-integrated Bingham plastic lower layer. A detailed description of this model is available in Skvortsov (2005). The initial slide volume is taken to be 2.7×10^7 m^3, which corresponds to the estimate in Murty (1979) for total mobilized volume and effectively includes the failed deltaic material as described in Prior et al. (1984). The entire event is initiated simultaneously, rather than sequentially as would be indicated by Prior et al. (1984). The resulting waves are significantly larger than indicated in reported visual observations, as discussed below. More recently, Fine and Bornhold (2011) have reported computational results which consider a Moon Bay slide occurring alone, without the associated deltaic failure, with volumes consistent with the estimate of Golder (1975). Fine and Bornhold (2011) obtain reasonable agreement with the observed wave height at First Nations Settlement using an idealized slide volume with a length of approximately 400 m, a maximum thickness of 34 m, and a total volume of 2.02×10^6m^3, in line with the earliest reported estimates by Golder (1975). Fine and Bornhold (2011) used a two-layer model similar to that used by Skvortsov and Bornhold (2007) but with a lower layer modeled as a viscous fluid with a range of viscosities from 2 to 20 kPa's this modeling approach is similar to the deformable slide formulation described below. No modeling results from previous studies are available for the southern portion

of Kitimat Arm including Clio Bay, and thus, it is not clear how previous model results compare to reported observations there.

Numerical approach

The numerical modeling conducted here is carried out using NHWAVE (Ma et al. 2012), a three-dimensional (3D) fully nonhydrostatic code, which is utilized to calculate surface displacement and velocity fields in response to either submarine or subaerial landslide events. NHWAVE retains a complete description of wave dispersion resulting from nonhydrostatic effects, and thus provides a more accurate description of frequency dispersion effects than the NLSWE models used previously (except in Thomson et al. 2012), but this addition was not found to lead to significant differences in modeled waves in the present case (owing to the short propagation distances involved relative to effective wavelength), and is not discussed further. The results presented below are based on the full nonhydrostatic model. The hydrostatic approximation can be recovered in the model by neglecting the forcing term S^p in Eq. (3).

Two modeling approaches are used here. In the first, ground motion resulting from slide or slump events is simulated assuming a solid sliding mass, using equations developed by Enet and Grilli (2007) to model the time history of slide motion. The second approach uses a depth-integrated lower layer representing a highly viscous Newtonian fluid (Fine and Bornhold 2011; Fine et al. 1994; Jiang and LeBlond 1992; Thomson et al. 2012). A previous use of NHWAVE together with a depth-integrated lower layer, but for the case of granular flow in slope-oriented coordinates over a simple planar bed, is shown in Ma et al. (2015).

Model for the water layer

NHWAVE solves Euler or RANS equations in 3D in a terrain and surface following σ coordinates defined by

$$x, y, \sigma = \frac{z+h}{D}, t \tag{1}$$

where (x, y, z) is the traditional Cartesian coordinate system with z oriented upwards against gravity and the still water surface lying in the (x, y) plane. Total water depth is given by $D(x, y, t) = h(x, y, t) + \eta(x, y, t)$, where h is the water depth from the still water level to the landslide surface, which is temporally varying during slide motion, and η is water surface elevation relative to still water. Depth h and surface displacement η are assumed to remain single-valued functions of (x, y) at all times.

Following Ma et al. (2012; 2015), well-balanced mass and momentum conservation equations in σ coordinates are given by

$$D_t + (Du)_x + (Dv_y) + \omega_\sigma = 0 \tag{2}$$

and

$$\boldsymbol{U}_t + \boldsymbol{F}_x + \boldsymbol{G}_y + \boldsymbol{H}_\sigma = \boldsymbol{S}^h + \boldsymbol{S}^p \tag{3}$$

where $\boldsymbol{U} = (Du, Dv, Dw)^T$, (u, v, w) are velocity components in (x, y, z) directions, and ω is the velocity normal to a level σ surface. Subscripts denote partial derivatives with respect to the indicated coordinate. The fluxes in the momentum equations are given by

$$\boldsymbol{F} = \begin{pmatrix} Duu + \frac{1}{2}g\eta^2 + gh\eta \\ Duv \\ Duw \end{pmatrix} \boldsymbol{G} = \begin{pmatrix} Duv \\ Dvv + \frac{1}{2}g\eta^2 + gh\eta \\ Dvw \end{pmatrix} \boldsymbol{H} = \begin{pmatrix} u\omega \\ v\omega \\ w\omega \end{pmatrix}$$

The source terms on the right-hand side of Eq. (3) are contributions from hydrostatic pressure and dynamic pressure, respectively. Turbulent diffusion terms have been neglected in this application, consistent with the derivation of a lower slide layer with a stress-free upper surface ("Depth-integrated slide layer"). These terms can be formulated as

$$\boldsymbol{S}^h = \begin{pmatrix} g\eta h_x \\ g\eta h_y \\ 0 \end{pmatrix} \quad \boldsymbol{S}^p = \begin{pmatrix} -\frac{D}{\rho^f}\left(p_x + p_\sigma \sigma_x\right) \\ -\frac{D}{\rho^f}\left(p_y + p_\sigma \sigma_y\right) \\ -\frac{1}{\rho^f} p_\sigma \end{pmatrix}$$

where p is the nonhydrostatic component of the pressure field and ρ^f is the water layer density.

Interaction between the landslide and water is accounted for using appropriate kinematic constraints on the velocity field and dynamic constraints which depend on the application. For the upper layer, the kinematic constraint is given by

$$w = -h_t - uh_x - vh_y z = -h \tag{4}$$

For the case of a moving solid slide, we neglect bottom shear stress acting on the water column and satisfy a linearized constraint on the pressure field given by Ma et al. (2012).

$$p_\sigma = \rho D h_{tt} \tag{5}$$

For the case of a viscous slide, we also neglect shear stresses at the slide surface (consistent with the form of the lower layer equation below) and impose continuity of total pressure P_h^f, given by

$$P_h^f = \rho^f g D + p \tag{6}$$

Kinematic constraints on the upper layer are also given by Eq. (4), while kinematic constraints on the slide layer are accounted for during depth integration of the equations for the slide. The two layers (water and slide) are completely coupled at each model time step.

Slides modeled as solid moving bodies

The geometry for slides considered here is specified according to the parameters defined in Fig. 2. We follow the approach of Enet and Grilli (2007) but make extensions to allow for the initial slide position to be either partially or entirely subaerial. We also

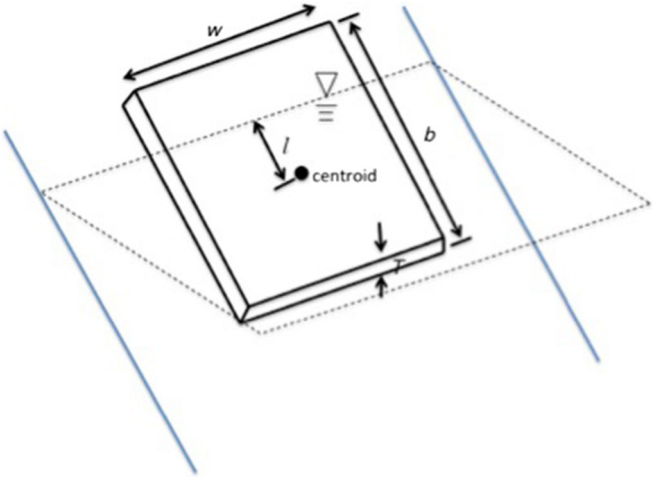

Fig. 2 Schematic of slide geometry for subaerial or submarine landslide

simplify the slide geometry to be a rectangular slab with thickness T, downslope length b, along-slope width w, total slide volume $V_s = bwT$, and total slide mass

$M_s = \rho_s V_s$, where ρ_s is the density of the slide material. We define a distance l as the downslope distance from the slab centroid to the waterline, which is assumed to be parallel to the slab edges, with l positive if the centroid is above the waterline. The relation between exposed, submerged, and total volumes V_{exp}, V_{sub}, V_s is then given by

$$\frac{V_{exp}}{V_s} = \frac{b/2 + l}{b}; \frac{V_{sub}}{V_s} = \frac{b/2 - l}{b} \tag{7}$$

Constructing a force balance (Enet and Grilli 2007) gives a second-order equation for downslope displacement $s(t - t_o)$ for a single slide

$$(b\gamma + C_m(b/2 - l))\ddot{s} = \left(b\gamma - \left(\frac{b}{2} - l\right)\right)(\sin\theta - C_n\cos\theta)g - \frac{1}{2}\left[C_d(b/2 - l) + C_f\frac{b/2 - l}{T}\right]\dot{s}^2; \quad s(t_o) = \dot{s}(t_o) = 0 \tag{8}$$

where t_o represents an arbitrary starting time, g is gravitational acceleration, $\gamma = \rho_s/\rho_w$, ρ_w is water density, C_d is a form drag coefficient, C_f is a skin friction coefficient, and θ is the bed slope in the direction of motion. In practice, γ is constrained by geotechnical properties and θ is constrained by the local bathymetry. The remaining free parameter in the formulation is the basal Coulomb friction coefficient $C_n = \tan\phi$, where ϕ is the Coulomb friction angle. The goals of the present study are to determine appropriate values of ϕ from model/data and model/model comparisons and to test the consistency of these results against experimental results reported in Sassa (1999).

In Eq. (2), appropriate limits occur when $l \to -b/2$, at which point the slab becomes completely submerged, recovering the model of Enet and Grilli simplified to the slab geometry, and $l \to b/2$, at which point the slab is completely exposed above the waterline and the effect of water-induced buoyancy and drag disappears from the governing equation.

Finally, the model has been extended to allow for the presence of multiple slide volumes V_{si} with independent start times t_{oi}.

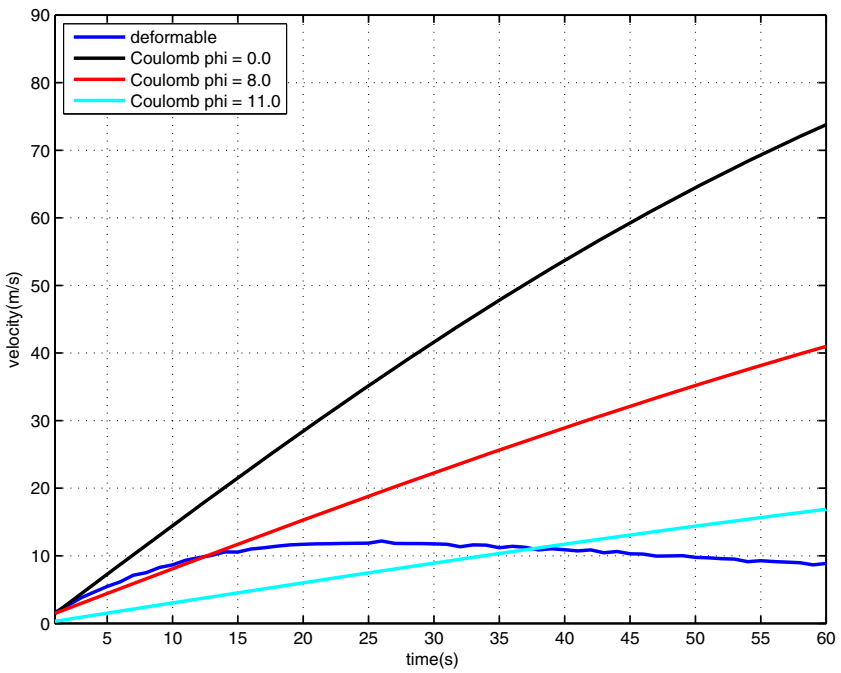

Fig. 3 Comparison of the centroid speed of the deformable slide model (*blue line*) with the slide velocity from the solid slide model with $\phi = 0^\circ$ (*black line*), $\phi = 8^\circ$ (*red line*), and $\phi = 11^\circ$ (*light blue line*)

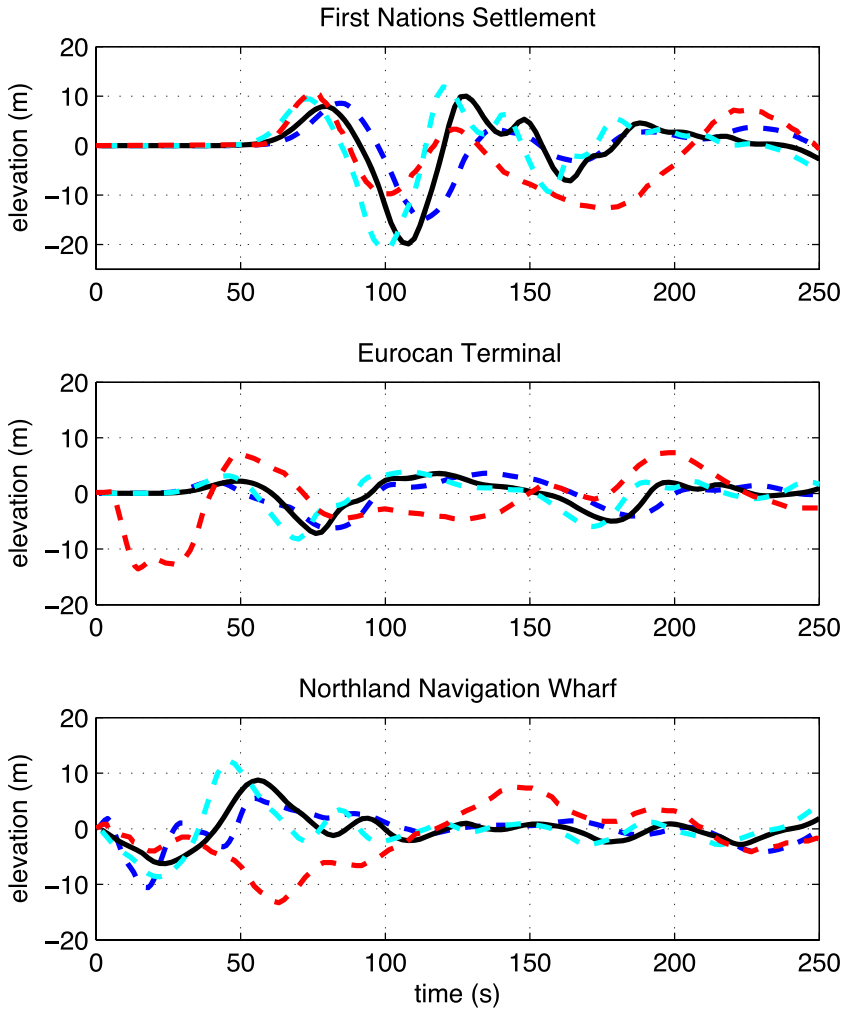

Fig. 4 Modeled surface elevations at First Nations Settlement, Eurocan Terminal, and Northland Navigation Wharf for a Moon Bay slide with $V_s = 2.7 \times 10^7$ m^3 and solid slides with $\phi = 0^\circ$ (*light blue dashed line*) and 8° (*solid black line*) and the viscous flow deformable model (*dark blue dashed line*) with $\mu = 10$ kPa. Results for the Bingham plastic model of Skvortsov and Bornhold (2007) (*red dashed line*) are taken from their paper and correspond to a different source geometry

Depth-integrated slide layer

Depth-integrated models for the lower slide layer have been formulated based on a number of rheologies, including Newtonian viscous fluid (Fine et al. 1994; Jiang and LeBlond 1992; Thomson et al. 2012), Bingham plastic (Jiang and LeBlond 1993; Skvortsov and Bornhold 2007), or granular masses (Kelfoun et al. 2010; Ma et al. 2015). In this study, we have used a slightly revised formulation for a viscous, Newtonian lower layer based on Fine et al. (1994), but with horizontal (normal stress) contributions to Newtonian stresses retained as in Jiang and LeBlond (1993). Formulating the equations in a quasi-conservative form based on slide layer thickness $d = h_s - h$ (where h_s is the depth from the still water surface to the fixed substrate below the slide) and horizontal volume flux $F = (dU, dV)$ (where U, V are depth-averaged horizontal velocities in the slide layer) gives

$$d_t + \nabla \cdot F - \epsilon \nabla^2 d = 0 \tag{9}$$

for mass conservation and

$$F_t + \frac{6}{5}\nabla_h \cdot (FF/d) = -gd\left[-\frac{\rho^s - \rho^f}{\rho^s}\nabla_h h + \frac{\rho^f}{\rho^s}\nabla_h \eta\right] - \frac{\mu}{\rho^s}\left(3\frac{F}{d^2} - \nabla_h^2 F\right) - \frac{gn^2}{d^{1/3}}\frac{F|F|}{d^2} \tag{10}$$

for momentum conservation, where ρ^s denotes slide density (here assumed to be constant) and ∇_h is a horizontal gradient operator. The quantity $\epsilon \nabla^2 d$ is a regularization term introduced for numerical purposes, $on = o(1)$, and it should be chosen such that the slide volume does not significantly decrease. Bottom friction is expressed through a quadratic stress term based on Manning's n.

Equation (9) is discretized using second-order centered differences. The momentum equation for the flux component dU (Eq. 10) employs a forward/backward difference approximation

Table 1 Observations and results of model simulations

		Maximum wave height (crest to trough), m	
		First Nations settlement	Clio Bay
Reported observations		7.6–8.2	6.1
Murty 1979		6.3–8.2	NA
Skvortsov and Bornhold 2007		~20	NA
Fine and Bornhold 2011		4.6–11.8	NA
Moon Bay	Test 1	9.80	1.60
	Test 2	8.19	1.25
	Test 3	6.92	1.03
	Test 4	9.65	1.60
	Test 5	9.50	1.55
Kitimat River delta	Test 6	3.80	2.35
	Test 7	6.70	5.35
	Test 8	6.60	6.90
Combined solid slides	Test 9	8.90	5.35
Combined deform. slides	Test 10	7.10	4.40

(depending on the sign of the slide velocity) with Δx^2 accuracy to discretize the divergence $\nabla_h \cdot (FF/d)$ in the x direction and central differences with Δy^2 accuracy to discretize the divergence term in the y direction. The momentum equation for the flux dV uses similar difference approximations, but with x and y swapped. Time stepping is carried out using the third-order Runge-Kutta method (Gottlieb and Shu 1998). The wetting-drying scheme for the moving slide boundary is identical to the approach of Nicolsky et al. (2011) applied to the NLSWE.

Hindcast of the 1975 Kitimat landslide tsunami

DEM development

Bathymetric data was obtained from the Canadian Hydrographic Service. The bathymetry data for Douglas channel is based on LON/LAT coordinates and MSL as the vertical datum. The data covers 53° 45′ 9″–53° 59′ 58″ north and 128° 56′ 18″–128° 38′ 59″ west. Data resolution is about 1/3″. The data was converted from LAT/LON to NAD 1983 BC Environmental Albers first and then interpolated onto a rectangular grid with 20 m × 20 m resolution.

The topography data covers Kitimat Arm and the adjacent areas of Douglas Channel including Clio Bay (Fig. 6) The data is based on NAD 1983 BC Environmental Albers with a resolution of about 100 m. The data was used to construct a rectangular grid with 20 m × 20 m resolution in the model domain. The bathymetric and topographic data were merged to construct the computational grid with a grid resolution of 20 m × 20 m.

Slide configurations

The first component of the 1975 event consists of a slide which was initiated in Moon Bay and slid primarily towards the east, consistent with the description in Golder (1975) and the modeled slide in Fine and Bornhold (2011). The slide is indicated in Fig. 1, with the initial location outlined by a solid red polygon. The slide is rectangular in plan, with geometric properties described in "Numerical approach." The slide has a specific gravity of $\gamma = 1.9$.

Prior et al. (1982a; 1982b; 1984) describe a large depositional structure running from north to south in Kitimat Arm, which they attribute to single or repeated failures of the Kitimat River deltaic structure. Prior et al. (1984) estimate that the homogeneous upper layer deposit in the structure, which may have been involved in the 1975 Kitimat tsunami event, has a volume up to 2.7×10^7 m^3. Since the smaller slide initiated in Moon Bay is seen below to not reproduce either the observed drawdown near the Eurocan terminal or the large wave further to the south in Clio Bay, we consider a second slide configuration consisting of slide volume originating in the area of the Kitimat River delta and moving along the longitudinal axis of Kitimat Arm, consistent with the configuration described in Prior et al. (1984).

Solid vs. deformable slides: parameterizing Coulomb friction

During initial tests of the model against previous computational results and observations, we conducted runs of the solid slide and deformable slide models using a single initial slide volume $V_s = 2.7 \times 10^7$ m^3, consistent with the volume estimate of Murty (1979) and as used by Skvortsov and Bornhold (2007) in their study using a Bingham plastic lower layer coupled to NLSWE for the water layer. In Skvortsov and Bornhold (2007), the slide volume is concentrated in the Moon Bay area and does not account for the original positioning of a large fraction of the volume in the Kitimat River delta formation. Consequently, the initial across-channel wave computed by Skvortsov and Bornhold (2007) is much larger in magnitude at the First Nations Settlement than indicated from observations, with a crest-to-trough wave height on the order of 20 m. We have used this configuration in order to examine consistency between the previous model and our own solid and deformable slide configurations.

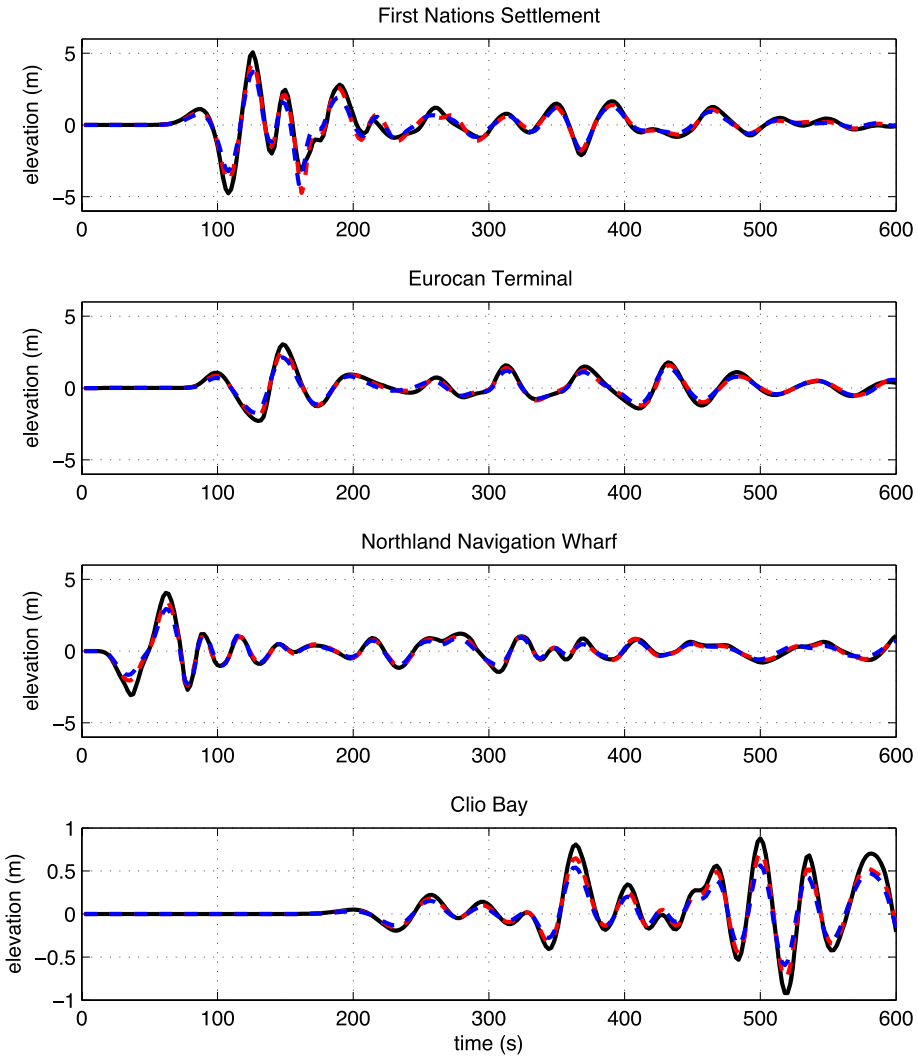

Fig. 5 Comparison of water surface elevations for varying slide volumes for the Moon Bay slide with fixed slide area. *Black solid lines*: $V_s = 2.329 \times 10^6$ m^3, *red dashed lines*: $V_s = 1.941 \times 10^6$ m^3, *blue dashed lines*: $V_s = 1.664 \times 10^6$ m^3

In previous numerical studies of tsunami generation using solid slides (Enet and Grilli 2007; Fuhrman and Madsen 2009; Ma et al. 2012), ϕ was usually set to zero in model validations using laboratory experiments. Here, we performed computations using the solid slide model described in "Slides modeled as solid moving bodies," using Coulomb friction angles of $\phi = 0^\circ$, corresponding to no basal friction, and $\phi = 8^\circ$, based on results compiled in Figure 8 of Sassa (1999). Calculations are also performed using the deformable slide model of "Depth-integrated slide layer" with a viscosity $\mu = 10$ kPa, consistent with the previous study of Fine and Bornhold (2011). Figure 3 shows a comparison of the centroid speed of the deformable slide model with the slide velocities from the solid slide model without Coulomb friction ($\phi = 0^\circ$) and with Coulomb friction ($\phi = 8^\circ$). (We choose centroid displacement as the main indicator of tsunamigenic potential following Grilli and Watts 2005). The figure shows that the solid slide model with $\phi = 8^\circ$ predicts slide velocities comparable to the deformable slide at the beginning of the slide motion, which is critical for accurate description of wave generation (Watts and Grilli 2003). We also show the slide motion for the choice of $\phi = 11^\circ$, which is used below for the smaller Moon Bay slide volume following Sassa's parameterization, but which clearly leads to an underprediction of the larger slide's displacement for the case considered here.

Figure 4 shows the time series of surface elevation obtained from the deformable slide model in comparison to the solid slide model with $\phi = 0^\circ$ and 8°. Results from Skvortsov and Bornhold (2007) are also shown for comparison. The figure shows that the model with $\phi = 0^\circ$ predicts higher wave crests at all three locations compared to both the model with $\phi = 8^\circ$ and the deformable model.

Moon Bay slide

We first consider the slope failure in Moon Bay in isolation, using the solid slide model. The slide volumes used here are in the neighborhood of 2×10^6 m^3, consistent with the estimates of volume presented by Golder Associates (Golder 1975) and used in Fine and Bornhold (2011). A Coulomb friction angle $\phi = 11^\circ$ is chosen, consistent with Sassa (1999).

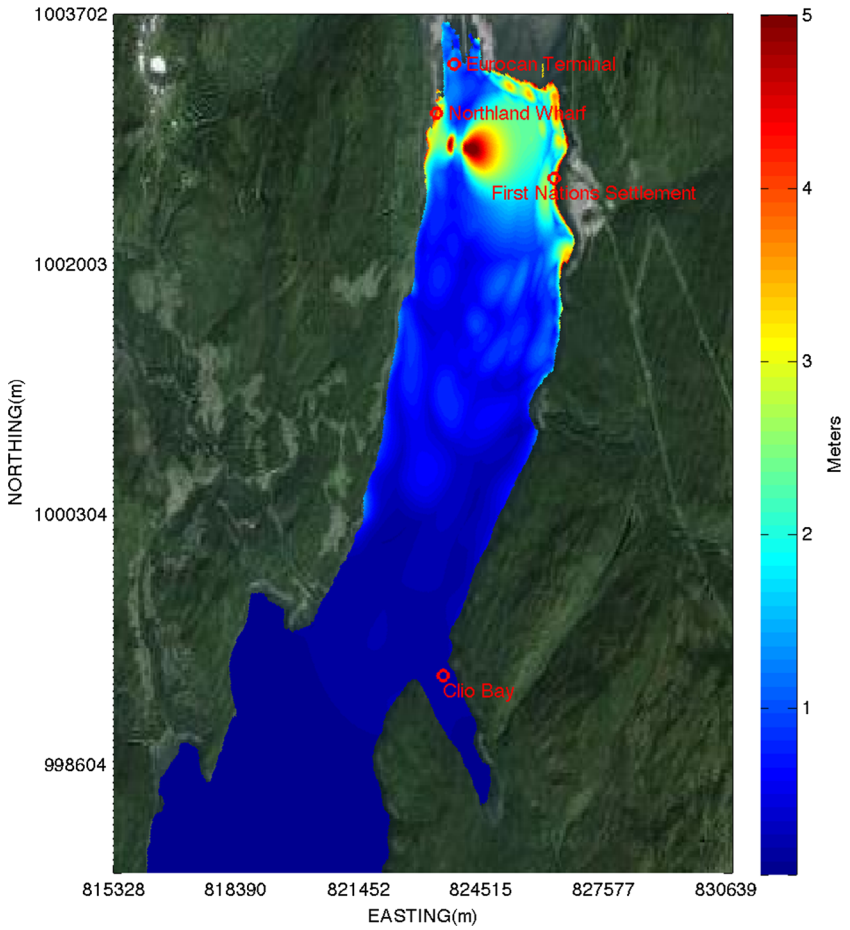

Fig. 6 Maximum amplitude of water surface displacement for Moon Bay slide. Test 1: $V_s = 2.329 \times 10^6$ m^3. Coordinates are NAD 1983 BC Environmental Albers

We first use a fixed slide area given by $b = 274.0$ m and $w = 250.0$ m and consider three cases of varying slide volume V_s, obtained by correspondingly varying slide thickness T. The tests are described by

Test 1: $V_s = 2.329 \times 10^6$ m^3, $b = 274.0$ m, $w = 250.0$ m, $T = 34$ m
Test 2: $V_s = 1.941 \times 10^6$ m^3, $b = 274.0$ m, $w = 250.0$ m, $T = 28.3$ m
Test 3: $V_s = 1.664 \times 10^6$ m^3, $b = 274.0$ m, $w = 250.0$ m, $T = 24.28$ m

The test 1 volume is close to that of the original estimate of Golder (1975), with tests 2 and 3 being 20 and 40 % smaller. Resulting maximum crest-to-trough wave heights are reported for these three cases in Table 1, and time series of the three events at the Kitimat First Nations Settlement, the Eurocan Terminal, Northland Navigation Wharf, and Clio Bay are shown in Fig. 5. The test 3 volume is close to the volume estimated from the bathymetric reconstruction carried out in Fine and Bornhold (2011), but is significantly smaller than the estimate of Golder (1975) and is smaller than is needed in Fine and Bornhold (2011) to get a good estimate of wave height at the First Nations Settlement, unless viscosity is set to a relatively low value. The test 2 slide volume $V_s = 1.941 \times 10^6$ m^3 produces a wave at First Nations Settlement which is closest to observations. This slide volume lies about midway between the Golder Associates estimate and the geometrical estimate of Fine and Bornhold. This volume is also close to the slide B volume reported in Fine and Bornhold (2011), which gave, in their study, a reasonable estimate for wave height at the First Nations Settlement using a viscosity of 10 kPa, consistent with our comparison to viscous deformable slide results in "Solid vs. deformable slides: parameterizing Coulomb friction." In general, wave heights at the First Nations Settlement, directly facing into the direction of slide motion, scale remarkably linearly with slide volume, with errors in scaling on the order of 1 %. This result breaks down somewhat in the far field, with wave height at Clio Bay for test 1 being about 60 % larger than that for test 3, compared to a 40 % increase in slide volume.

Figure 6 shows a plot of the maximum occurring positive water surface elevation at each location in the computational domain for test 1. The event is localized to the near field shoreline, the locus of the sliding mass, and the facing shorelines to the east and north. In particular, this configuration of the total event predicts very little impact in the area of the Eurocan terminal, and produces no wave traveling to the south that would be of sufficient magnitude to explain observations in Clio Bay. Water surface fluctuations in the

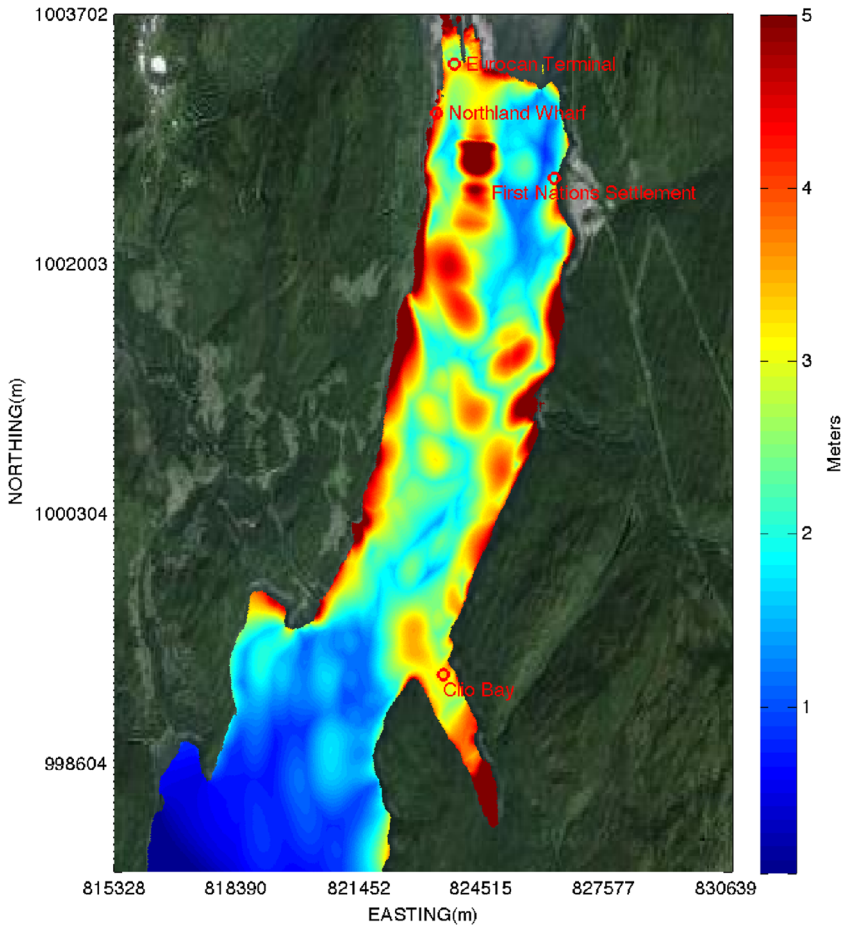

Fig. 7 Maximum positive water surface displacement in meters. Kitimat River delta slide, $V_s = 2.0 \times 10^7$ m^3. Coordinates are NAD 1983 BC Environmental Albers

northern portion of Kitimat Arm are also predicted to die out quickly, and do not exhibit the observed, persistent motion reported by eyewitnesses.

Two additional tests for the Moon Bay slide were carried out using the test 1 slide volume but with varying slide width and thickness, giving slide widths increased by 20 and 40 %. The tests are described by:

Test 4: $V_s = 2.329 \times 10^6$ m^3, $b = 274.0$ m, $w = 300.0$ m, $T = 28.3$ m
Test 5: $V_s = 2.329 \times 10^6$ m^3, $b = 274.0$ m, $w = 350.0$ m, $T = 24.3$ m

These changes represent slides with greatly increased width but constant cross-sectional area perpendicular to the direction of motion. Results in Table 1 show very little variation in reported wave heights in the near or far fields; corresponding plots of results are omitted.

Kitimat River delta slide

We next consider a simulation of a failure located initially on the Kitimat River delta, outlined in blue in Fig. 1. Three tests were conducted using slide volumes which fall at the extreme of the range of reported estimates of slide deposits along the Kitimat Arm bottom which are thought to be the result of the 1975 event. The corresponding model parameters for the tests are:

Test 6: $V_s = 1.0 \times 10^7$ m^3, $T = 10.0$ m, $b = 1000.0$ m, $w = 1000.0$ m
Test 7: $V_s = 2.0 \times 10^7$ m^3, $T = 20.0$ m, $b = 1000.0$ m, $w = 1000.0$ m
Test 8: $V_s = 2.7 \times 10^7$ m^3, $T = 22.1$ m, $b = 1105.0$ m, $w = 1105.0$ m

Coulomb friction angles for these cases are taken to be $\phi = 8^\circ$ (Sassa 1999).

The waveform generated here is lower in frequency and longer in wavelength than the Moon Bay baseline case slide, and the slide orientation is effective in generating a wave moving along the axis of Kitimat Arm, with significant wave heights occurring to the south. A map of maximum occurring water surface displacements is shown in Fig. 7 for the test 7 results. The maximum impact of this event is concentrated more directly around the Eurocan Terminal area and along the shorelines to the south, with impacts at the Northland Navigation Wharf and First Nations Settlement falling below the level produced by the much smaller Moon Bay

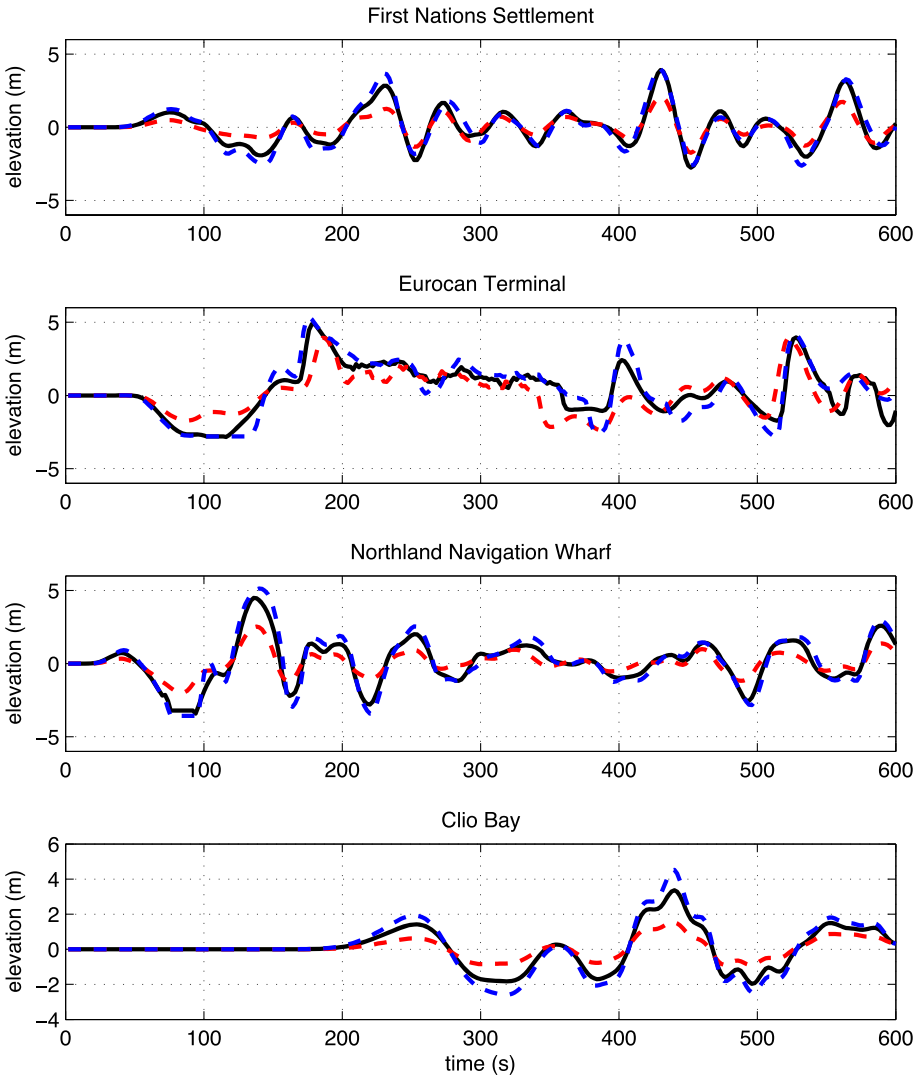

Fig. 8 Time series of water surface displacements in meters for tests 6 ($V_s = 1.0 \times 10^7$ m^3, *red dashed line*), 7 ($V_s = 2.0 \times 10^7$ m^3, *black solid line*), and 8 ($V_s = 2.7 \times 10^7$ m^3, *blue dashed line*). Kitimat River delta slide

slide. Time series for the Kitimat River delta slide cases are shown in Fig. 8, and maximum wave height values are reported in Table 1.

The two larger slides (tests 7 and 8) cause a significant initial drawdown and exposure of the bottom in both the Eurocan Terminal and Northland Navigation Wharf areas, consistent with observations reported by Murty and Brown (1979). The smaller of the three slides (test 6) does not expose the bottom in either of these regions, indicating that it is likely to be too small. Secondly, the event does not create a disturbance at First Nations Settlement in excess of the Moon Bay slide. The lower-frequency motions continue to reverberate in the northern portion of Kitimat Arm, consistent with the observation that motions from the event persisted for up to an hour. Finally, the event produces a maximum wave height at Clio Bay of 5.35 m, somewhat lower than reported (from visual observations by a boater). The lower amplitude wave at Clio Bay produced in test 6 again indicates that the estimate of slide volume $V_s = 1.0 \times 10^7$ m^3 is probably too small.

For the three slide volumes tested, results for wave heights in the far field (i.e., Clio Bay) are seen to scale approximately linearly with slide volume. The larger of the slide volumes produces an estimate of wave height at Clio Bay which is likely too large, given that the estimate of wave height of 6.2 m obtained by the boater in the area is likely to be high. In contrast, the larger slide does not produce uniformly scaled-up results in the northern part of Kitimat Arm, possibly due to a number of effects including the extreme nonlinearity of the event (with pronounced bottoming out of the harbor region around the Eurocan Terminal), the complex wave pattern resulting from the short travel time and multiple reflections in the area, and the fact that the initial wave is largely directed away from the reported First Nations Settlement site.

Superposition of Moon Bay and Kitimat River delta slides

The results presented so far have indicated that neither slide configuration alone provides a completely satisfying reproduction of all observed features of the event, and it is of interest to examine a combination of the two. In this section, we compare results obtained by linearly superimposing test 2 and test 7 results for Moon Bay and Kitimat River delta

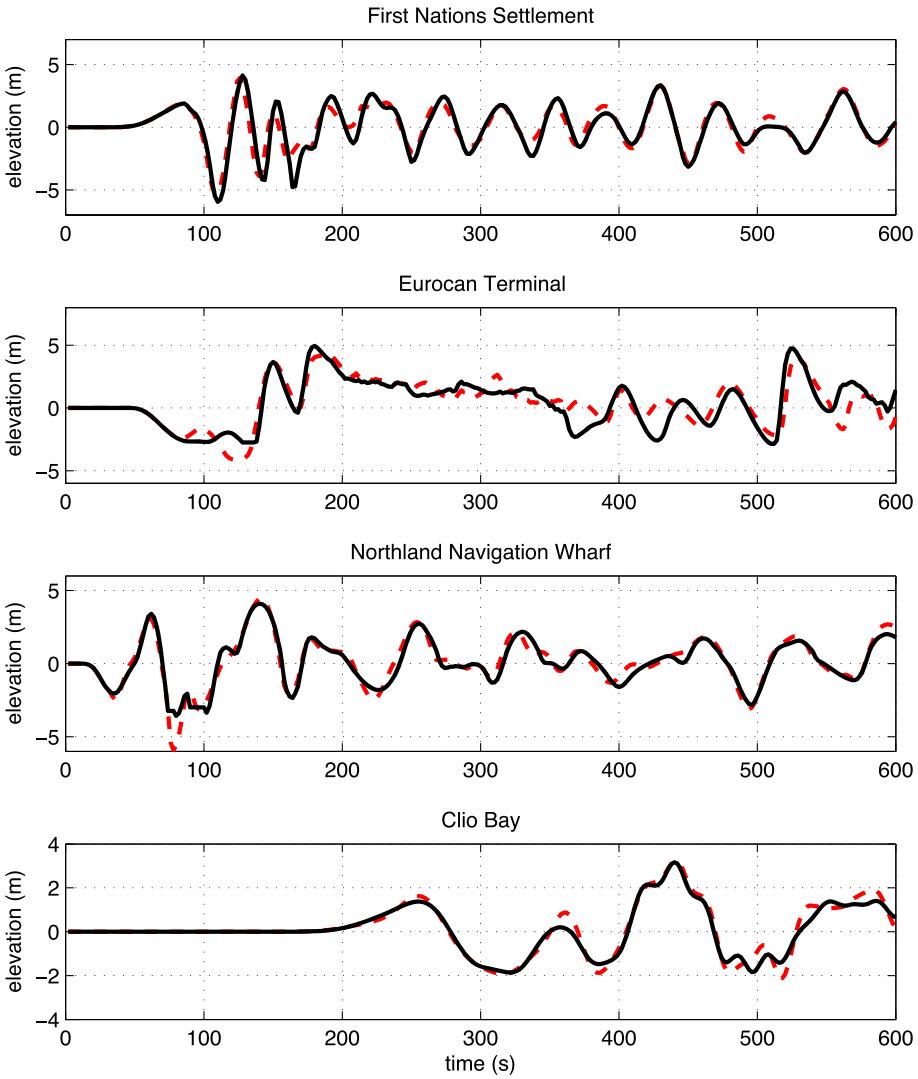

Fig. 9 Comparison of water surface elevations for the multi-slide model (test 9: *black solid line*) with the linear superposition of water surface elevation (*red dashed lines*) from the Moon Bay slide ($V_s = 1.941 \times 10^6$ m^3, test 2) and Kitimat River delta slide ($V_s = 2.0 \times 10^7$ m^3, test 7)

slides, respectively, with results for a simulation which combines the two ground motions in a single simulation (test 9). Johns et al. (1986) have suggested that the timing difference between the two slides would possibly be based on the time required for the failed slide material from Moon Bay to arrive at the delta front, but this suggestion has not been examined in more detail and would strongly depend on the choice of the two slide geometries in our simulations. We have thus not accounted for this difference based on travel time in the present study. A plot of the superposition of results for tests 2 and 7 is shown in Fig. 9 as the red dashed line. The combined events provide a more comprehensive agreement with published observations. The dominance of the Moon Bay slide in the west to east direction in determining maximum water surface displacement at the First Nations Settlement is preserved, while the additional observations of strong drawdown in the harbor and large waves further to the south are accounted for by the addition of the second larger Kitimat River delta slide failure in the north to south direction.

Test 9 results (Fig. 9, solid line) for the combination of the two slides in a single simulation show that linear superposition is largely valid for the event, except in areas where tsunami surface displacements are of the order of the local depth. The validity of the linear superposition is undoubtedly due to the great depth of the Kitimat Arm fjord, which renders the wave height-to-water depth ratio controlling nonlinearity to be small. The exception to this occurs during maximum drawdown at the Eurocan Terminal and the Northland Navigation Wharf, where the linearly superposed drawdowns exceed the local water depth.

Deformable viscous slide

A deformable slide simulation (test 10) was carried out for the combined slide configuration, using the viscous layer slide model. The initial slide geometry is a combination of the Moon Bay slide (test 2) and the Kitimat River delta slide (test 7), with both slides initiated simultaneously. A fluid viscosity of 10 kPa is used for the lower slide mass in all simulations.

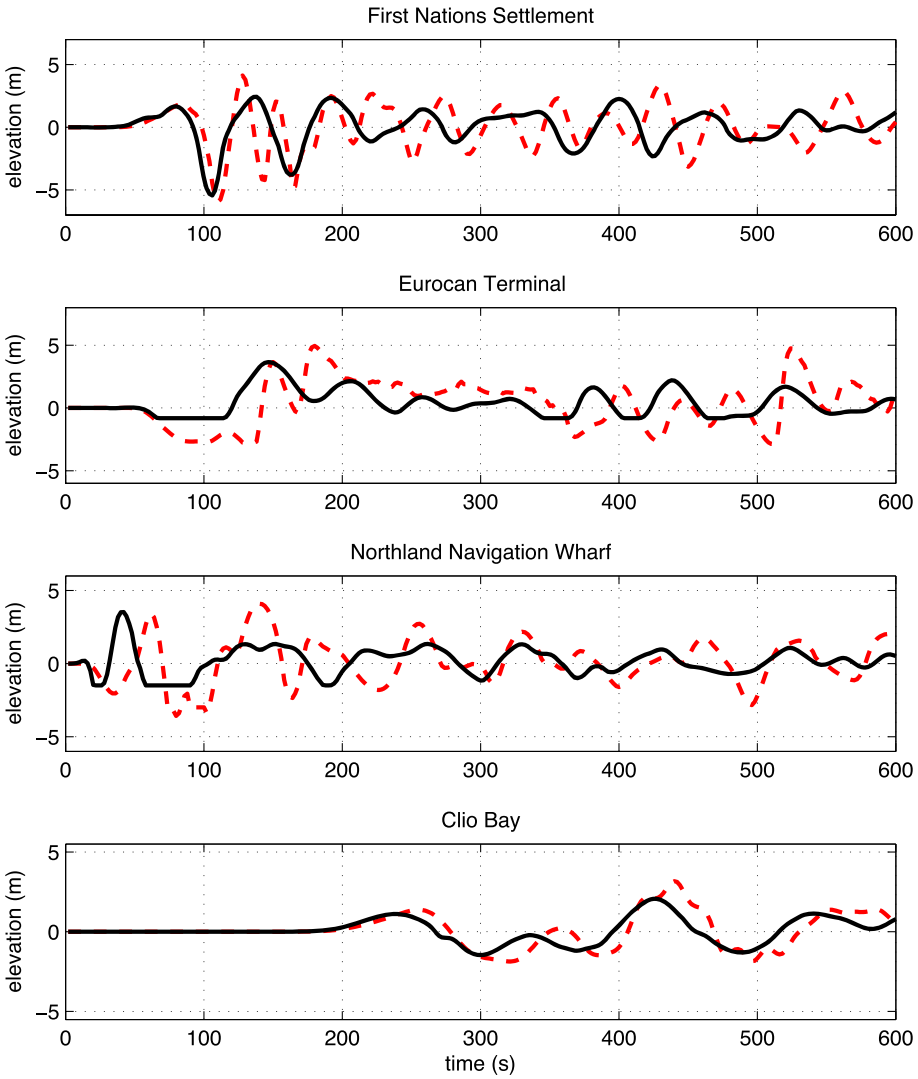

Fig. 10 Comparison of water levels resulting from solid slide superposition (*red dashed lines*) and a deformable slide simulation (*black solid lines*)

A comparison of the deformable slide results to the superposed solid slide results from test 9 is shown in Fig. 10. Note that the reduction of drawdown at the Eurocan Terminal and the Northland Navigation Wharf in the deformable slide case is an artifact of the initial slide deformation, which includes an upslope as well as a downslope collapse, effectively infilling several of these shallow regions. No detailed attempts have been made to configure the initial geometry of the viscous slide in order to eliminate this upslope collapse, as our main interest is in the wave-making performance of the two models relative to each other.

Test 9 and test 10 results are largely consistent in terms of maximum generated wave heights, but the deformable slide produces a wave form with less high-frequency content in the near field of the event. These types of model discrepancies would be a strong basis for discriminating between models in a well-constrained experimental setting, but the knowledge of the source mechanism and geometry in the present case would not allow such an evaluation. The differences in frequency content in the near field are largely absent once the waves have propagated to Clio Bay. The overall comparison indicates that the deformable slide model predicts somewhat lower wave heights than the solid slide model. Existing data is insufficient as a basis for drawing more detailed conclusions on the accuracy of the results.

Discussion

The smaller Moon Bay slides considered here (tests 2 and 3; Table 1) produce crest-to-trough wave amplitudes at the First Nations Settlement site which are consistent with the observations reported in Golder (1975), Murty (1979), and Murty and Brown (1979). In particular, a Moon Bay slide with a volume of $V_s = 1.941 \times 10^6$ m^3 is seen to produce a wave height at First Nations Settlement of 8.2 m, in close agreement with the published observations (Table 1, test 2). This slide is slightly larger than the initial reconstructed slide volume from

Fine and Bornhold (2011) and 14 % smaller than the initial estimate of 2.3×10^6 m^3 reported by Golder (1975). Wave heights resulting from slide volumes at either end of that range are still reasonable and consistent with observations to within a reasonable degree of uncertainty. It was found that the wave height at First Nations Settlement is not sensitive to reasonable changes in the initial solid slide width, with total slide volume held constant. It is apparent that this reconstruction of the main west to east slide, with volumes in reasonable agreement with reconstructions of the slide volume based on examination of bathymetric data (Fine and Bornhold 2011; Golder 1975), provides a description of wave height at First Nations Settlement which is consistent with observations. In our simulation, the arrival time of the largest positive crest occurs about 120 s after the initiation of the slide event. The Moon Bay slide scenario considered here does not reproduce additional observations, including the occurrence of a large-amplitude wave with height on the order of 6 m, further to the south in Clio Bay, and the large drawdown of water level occurring early in the event in the Eurocan terminal and other areas in the northern extreme of the Arm. A second slide representing a failure of the Kitimat River delta structure is seen to reproduce these observations without interfering with the Moon Bay slide as the dominant mechanism for the largest wave at First Nations Settlement.

Overall, the model has been shown to produce tsunami wave heights which are consistent with previous modeling efforts, and has further been shown to give reasonable predictions of observed wave activity when used in a manner that is consistent with the present understanding of the event. Model results indicate that the strongest influence on the amplitude of generated waves is the slide volume, with changes in slide shape (with volume held constant) playing a lesser role. The model is sensitive to the choice of internal Coulomb friction angle ϕ for the solid slide case, but this choice may be constrained using estimates of ϕ shown in Sassa (1999), Figure 8, leading to results which are in reasonable agreement with observations. In particular, waves generated using solid slides with ϕ constrained by Sassa (1999) are of comparable magnitudes to waves generated using deformable slides with fluid viscosities comparable to values obtained in the calibration reported in Fine and Bornhold (2011), given equal slide volumes. Further, as shown in Table 1, the maximum wave height observations at the First Nations Settlement and Clio Bay fall within the modeling results obtained from the superposition of Moon Bay and Kitimat River delta slides, using either the solid or deformable slide models.

The viscous flow model described here represents the initial stage in the development of a depth-integrated slide layer coupled to the general nonhydrostatic 3D code NHWAVE for free-surface hydrodynamics. The modeled material rheology is presently being extended to include granular debris flow (Ma et al. 2015), erosion and deposition of substrate material, entrainment of water from the overlying water layer, and effects of vertical acceleration which are neglected in the present and earlier formulations for the slide layer in horizontal Cartesian coordinates. These developments will be reported in the near future.

Acknowledgments

This work was partially supported by Grant CMMI-1537568 from the Engineering for Natural Hazards Program, National Science Foundation, to the University of Delaware. Kirby, Shi, and Nicolsky acknowledge the continuing support of the National Tsunami Hazard Mitigation Program, NOAA.

References

Bornhold BD, Thomson RE, Rabinovich AB et al. (2001) Risk of landslide-generated tsunamis for the coast of British Columbia and Alaska. In: 2001 An earth odyssey. Int Assoc Hydrogeolo 1450–1454

Bornhold BD, Harper JR, McLaren D, Thomson RE (2007) Destruction of the First Nations village of Kwalate by a rock avalanche-generated tsunami. Atmosphere-Ocean 45(2):123–128. doi:10.3137/ao.450205

Enet F, Grilli ST (2007) Experimental study of tsunami generation by three-dimensional rigid underwater landslides. J Waterw Port Coast Ocean Eng 133(6):442–454

Fine I, Bornhold B (2011) Submarine landslide-tsunami modeling, April 27, 1975. Appendix F in Landslide-generated wave hazard analysis, Kitimat Arm, Enbridge Northern Gateway Project. Tech. rep., AMEC

Fine IV, Rabinovich AB, Kulikov EA et al. (1998) Numerical modelling of landslide-generated tsunamis with application to the Skagway Harbor tsunami of November 3, 1994. Int Conf Tsunamis

Fuhrman DR, Madsen PA (2009) Tsunami generation, propagation, and run-up with a high-order Boussinesq model. Coast Eng 56:747–758. doi:10.1016/j.coastaleng.2009.02.004

Golder Associates (1975) Report to B. C. Water Resources Service in investigation of seawave at Kitimat B.C. Tech. Rep. V75077, Golder Associates

Gottlieb S, Shu CW (1998) Total variation diminishing Runge Kutta schemes. Math Comput 67:73–85

Grilli ST, Watts P (2005) Tsunami generation by submarine mass failure. I: modeling, experimental validation, and sensitivity analysis. J Waterw Port Coast Ocean Eng 131(6):283–297. doi:10.1061/(ASCE)0733-950X(2005)131:6(283)

Jiang L, LeBlond PH (1992) The coupling of a submarine slide and the surface waves which it generates. J Geophys Res 97(C8):12,731–12,744

Jiang L, LeBlond PH (1993) Numerical modeling of an underwater Bingham plastic mudslide and the waves which it generates. J Geophys Res 98(C6):10,303–10,317

Johns MW, Prior DB, Bornhold BD, Coleman JM, Bryant WR (1986) Geotechnical aspects of a submarine slope failure, Kitimat Fjord, British Columbia. Mar Geotechnol 6:243–279

Kelfoun K, Giachetti T, Labazuy P et al. (2010) Landslide-generated tsunamis at Réunion Island. J Geophys Res 115(F04012), doi: 10.1029/2009JF001381

Kulikov EA, Rabinovich AB, Thomson RE, Bornhold BD (1996) The landslide tsunami of November 3, 1994, Skagway Harbor, Alaska. J Geophys Res 101(C3):6609–6615

Ma G, Shi F, Kirby JT (2012) Shock-capturing non-hydrostatic model for fully dispersive surface wave processes. Ocean Model 43–44:22–35. doi:10.1016/j.ocemod.2011.12.002

Ma G, Kirby JT, Hsu TJ, Shi F (2015) A two-layer granular landslide model for tsunami wave generation: theory and computation. Ocean Model 93:40–55. doi:10.1016/j.ocemod.2015.07.012

Miller DJ (1960) The Alaska earthquake of July 10, 1958: giant wave in Lituya Bay. Bull Seismol Soc Am 50:253–266

Murty TS (1979) Submarine slide-generated water waves in Kitimat Inlet, British Columbia. J Geophys Res 84(C12):7777–7779

Murty TS, Brown RE (1979) Kitimat Inlet and the water waves that accompanied the slide. Pacific Marine Science Report 79-11. Institute of Ocean Sciences, Patricia Bay, Sidney

Nicolsky DJ, Suleimani E, Hansen R (2011) Validation and verification of a numerical model for tsunami propagation and runup. Pure Appl Geophys 168:1199–1222. doi:10.1007/s00024-010-0231-9

Prior DB, Bornhold BD, Coleman JM, Bryant WR (1982a) Morphology of a submarine slide, Kitimat Arm, British Columbia. Geology 10:588–592

Prior DB, Coleman JM, Bornhold BD (1982b) Results of a known seafloor instability event. Geo-Mar Lett 2:117–122

Prior DB, Bornhold BD, Johns MW (1984) Depositional characteristics of a submarine debris flow. J Geol 92(6):707–727

Rogers GC (1980) A documentation of soil failure during the British Columbia earthquake of 23 June, 1946. Can Geotech J 17:122–127

Sassa K (1999) Landslide volume—apparent friction relationship in the case of rapid loading on alluvial deposits. In: Sassa K (ed) Landslides of the world. Tokyo University Press, Tokyo

Skvortsov A (2005) Numerical simulation of landslide-generated tsunamis with application to the 1975 failure in Kitimat Arm, British Columbia, Canada. Master of science, University of Victoria, School of Earth and Ocean Sciences

Skvortsov A, Bornhold B (2007) Numerical simulation of the landslide-generated tsunami in Kitimat Arm, British Columbia, Canada, 27 April 1975. J Geophys Res 112(F02028), doi: 10.1029/2006JF000499

Thomson RE, Fine I, Krassovski M et al. (2012) Numerical simulation of tsunamis generated by submarine slope failures in Douglas Channel, British Columbia. Tech. Rep. Research Document 2012/115, Canadian Science Advisory Secretariat

Watts P, Grilli ST (2003) Underwater landslide shape, motion, deformation, and tsunami generation. In: Proc 13th ISOPE, Honolulu 364–371

J. T. Kirby (✉) · F. Shi
Center for Applied Coastal Research, Department of Civil and Environmental Engineering,
University of Delaware,
Newark, DE 19716, USA
e-mail: kirby@udel.edu

D. Nicolsky
Geophysical Institute,
University of Alaska Fairbanks,
903 Koyokuk Drive, Fairbanks, AK 99775, USA

S. Misra
Chevron Energy Technology Company,
1400 Smith St., Houston, TX 77002, USA